Microelectronic Engineering 111 (2013) 396–403

Contents lists available at SciVerse ScienceDirect

Microelectronic Engineering

journal homepage: www.elsevier.com/locate/mee

Quantitative analysis of hepatic cell morphology and migration in response to nanoporous and microgrooved surface structures

K.Y. Mak [a], L. Li [a], C.M. Wong [b,c], S.M. Ng [d], C.W. Leung [d,*], J. Shi [e], H.K. Koon [e], X. Chen [e], C.S.K. Mak [f], M.M. Chan [g], P.W.T. Pong [a,*]

[a] Department of Electrical and Electronic Engineering, The University of Hong Kong, Hong Kong
[b] Department of Pathology, The University of Hong Kong, Hong Kong
[c] State Key Laboratory for Liver Research, The University of Hong Kong, Hong Kong
[d] Department of Applied Physics, Hong Kong Polytechnic University, Hong Kong
[e] Department of Physics, Hong Kong Baptist University, Hong Kong
[f] Department of Chemistry, The University of Hong Kong, Hong Kong
[g] Department of Surgery, University of Cambridge, United Kingdom

ARTICLE INFO

Article history:
Available online 16 April 2013

Keywords:
Hepatic cell line
Nanopores
Microgrooves
Cell morphology
Cell migration

ABSTRACT

Material surface topography is an important factor for regulating cellular behaviour. Understanding the mechanism of how surface topography influences mammalian cells is critical for the development of medical implants and tissue engineering. In this study, we investigated the influences of nanoporous and microgrooved substrates on the morphology and migration of hepatic cell line, BEL-7402 cells. Cells were cultured on nanoporous (140 nm in diameter) anodized alumina membrane (AAM), nanoporous (140 nm in diameter) polydimethylsiloxane (PDMS), and microgrooves (10 μm, 30 μm, and 50 μm in width, and 2 μm in depth) patterned PDMS, then imaged by fluorescent microscopy, time-lapse microscopy, and scanning electron microscopy (SEM). Cell morphology and migration were investigated through image analysis. The results suggest that the nanoporous and microgrooved surface structure induced totally different changes on BEL-7402 cells. Compared to the well-spread cells on the flat surface plate, the cells formed spheroids on the nanoporous AAM surface and nanoporous PDMS surface with no elongation and alignment, while the cells grew with elongated and aligned morphology along the microgrooves on the PDMS substrates. The BEL-7402 cell migration speed was significantly higher on the nanoporous substrates than on the flat surfaces. On the microgrooved PDMS substrates, the cells migrated along the groove direction and showed relatively small difference of the overall velocity compared to the cells on the flat PDMS surface. Our findings provide insights into the control of cell morphological features and migratory behaviour by using artificial nanoporous or microgrooved substrates, which can benefit the research on hepatocellular carcinoma metastasis, tissue engineering, and medical implant design.

1. Introduction

Mammalian cells in vivo are exposed to a complex, textured, porous, and structured environment. The porosities and topographies of cellular environment extend at all scales from macro to nano [1]. It is believed that the micro-scale and sub-micro-scale surface structures of extracellular matrix (ECM) are a critical parameter in guiding cell morphology and migratory behaviour in several situations [2,3]. It is also reported that the nano-porosity of sinusoidal endothelium might be related to the invasion of hepatocellular cells [4]. Therefore, the cells encounter and respond to topography in the in vivo environment at micro/nano-scales. Inspired by these discoveries, artificial micro-/nano-structured surfaces have attracted enormous interest to be used as bio-mimic environments for medical applications such as tissue engineering. Among these artificial micro-/nano-structured surfaces, alumina, and PDMS are two most commonly used materials as culture substrates because of their biocompatibilities.

Although a variety of cell types have been used in cell-substrate studies for different purposes, hepatic cells have just started to gain attention recently [5–7]. Hoess et al. successfully used the nanoporous alumina for the co-cultivation of mesenchymal stem cells and primary hepatocytes [8], which can be used in fabricating microcapsule for hepatocyte in non-autologues cell therapy to prevent adverse immune response. Eckert et al. suggested that alumina ceramics can be used to fabricate cell carrier for in vivo tissue replacement [9]. In addition, Leclerc et al. demonstrated the cultivation of fetal human hepatocytes in microstructured PDMS [10]. PDMS were also used to develop bioartificial liver reactor in

* Corresponding authors.
E-mail addresses: dennis.Leung@inet.polyu.edu.hk (C.W. Leung), ppong@eee.hku.hk (P.W.T. Pong).

0167-9317/$ - see front matter © 2013 Elsevier B.V. All rights reserved.
http://dx.doi.org/10.1016/j.mee.2013.04.009

culturing hepatocyte in vitro [11,12], and may function as a bridge to liver transplant or as a short-term liver-assisting device with adequate anticoagulation and antiplatelet agents [13]. In the scope of further applying nano-structured alumina and micro-structured PDMS in the field of liver tissue engineering, it is necessary to carefully investigate the cell-substrate interactions between micro-/nano-structured alumina/PDMS and hepatic cells.

It was previously shown that the dimension and distribution of the grooves or pores on the micro-/nano-structured surfaces have important influences on cellular behaviour. For example, the nanoporous surface can enhance the cell adhesion of osteoblasts [14,15]. The width of the microgrooved structure can regulate the cell alignment and cell morphology of human mesenchymal stem cells [16]. In this study, we investigated the effects of artificial nanoporous and microgrooved surfaces on hepatic cellular behaviour. BEL-7402, derived from human hepatoma, retains epithelial cell like features and morphology and shows some specific biochemical functions of hepatocytes [17]. Since the BEL-7402 cell line is immortal and resistant to the cryopreservation, the usage of BEL-7402 offers advantages compared to the primary liver cells in terms of availability, growth activity, and quality control [18]. Thus, the cell line BEL-7402 was adopted in this study to evaluate the effects of nanoporous/microgrooved surfaces on hepatic cells. The BEL-7402 cells were cultured on flat cell culture plate, flat alumina surfaces, nanoporous AAM (140 nm in diameter), flat PDMS, and microgrooved PDMS surfaces patterned by micro-contact printing (10 μm, 30 μm, or 50 μm width, and the periodicity is twice the groove width). Cellular behaviour on these surfaces was observed using fluorescence microscopy, time lapse microscopy, and scanning electron microscopy (SEM). The cell morphology and cell migration on these surfaces were analyzed through cell spreading area, cell elongation, cell alignment, and cell migration speed.

2. Experiments

2.1. Substrate preparation

AAMs with pore size of 140 nm were purchased from Pu-Yuan Nano Technology (China). The flat alumina surfaces, used as control, were fabricated by sputtering coverslips and flat silicon wafers with alumina by RF magnetron sputtering. The presence of alumina layer on the control alumina surfaces was confirmed by energy-dispersive X-ray spectroscopy (EDX). Patterned PDMS substrates were prepared using standard micro-contact printing technique. First, silicon masterboards were prepared with a negative pattern to be imparted onto the PDMS. Next, the two part silicone presursors (SYLGARD 184, Down Corning) was mixed in a 10:1 ratio. The mixture was poured onto a Si masterboard with predefined patterns and kept in air for several hours. After degassing, it was cured at 65 °C for at least 30 min. The solidified PDMS was then peeled off, transferring the pattern from Si masterboard onto the PDMS soft replica. The periodicities of the microgrooves were twice the groove widths. All substrates were submerged and sterilized in 70% ethanol aqueous solution, followed by rinsing with PBS before surface characterization and cell culturing.

2.2. Cell culture

The BEL-7402 cells were obtained from the Cell Institute, Sinica Academica Shanghai, Shanghai, China. The cells were then virally transduced with green fluorescence protein (GFP) DNA. GFP was applied for image enhancement when the cells were observed through semi-transparent substrates such as the nanoporous AAM. The BEL-7402 cells were cultured in DMEM-HG supplemented with 10% fetal bovine serum (FBS), 100 U/ml penicillin, and 100 μg/ml streptomycin, at 37 °C and 5% CO_2 in a humidified incubator.

2.3. SEM observation

Cells were seeded onto the different surfaces at a concentration of 1×10^5 cells/ml, and were allowed to attach to the substrates for 24 h. Next, the cells were rinsed with cacodylate buffer and were fixed with 2.5% glutaraldehyde for 30 min at room temperature. The samples were dehydrated in a series of ethanol rinses (25%, 50%, 70%, 90%, and 100%) and critical-point dried (Bal-tec CPD030 critical point dryer). 5 nm gold and gallium were then coated onto the samples by sputtering (Bal-Tec SCD005 sputter coating) before SEM characterization (Hitachi S-4800 FEG SEM). Image analyses were carried out with a home-made image analysis software and ImageJ.

2.4. Time-lapse microscopy

BEL-7402 cells were seeded on the nanoporous AAM and the microgrooved PDMS in the presence of CO_2 independent culture medium (Invitrogen) supplemented with 10% FBS, 100 U/ml penicillin, and 100 μg/ml streptomycin. The cells were observed using an inverted microscope (Nikon ECLIPSE Ti) enclosed in a humidified 37 °C chamber. Images were taken every 10 min by using a motorized stage and analyzed by the Metamorph (Molecular Devices) software package.

Since the nanoporous AAM is semi-transparent, the cell morphology on the AAM could not be viewed clearly under the inverted optical microscope in bright field. Twenty-four hours after the initial cell seeding on AAM nanopores, fluorescent images were captured every 10 min up to 4 h using fluorescence time-lapse microscopy. Twenty-four hours after the initial cell seeding on the micro-grooved PDMS, phase contrast images were captured every 10 min up to 4 h using bright field time-lapse microscopy. The flat cell culture plate, flat alumina surface, and flat PDMS were used as the control substrates.

2.5. Characterization of cell morphology

Cells that made no contact with neighboring cells were selected and analyzed with ImageJ [19]. Based on the optical images, the outlines of cells were traced manually and the enclosed areas were calculated as the cell spreading area. Each cell was further fitted to an ellipse. The elongation of the cell is defined as the ratio of the corresponding ellipse major/minor axis length. The alignment of the cells on the PDMS microgrooves was represented by the average orientation angle (0–90°) between the major axis of the corresponding ellipse and the direction of the microgrooves [20].

2.6. Cell migration study

The cell centroids were determined manually and the mean centroid displacement per unit time was subsequently calculated using ImageJ. The x and y axes were considered as parallel and perpendicular to the grooves direction, respectively. Average velocity was calculated for each cell between consecutive time points by the following formulas:

Parallel velocity

$$v_x(t) = \frac{\Delta x(t)}{\Delta t} \tag{1}$$

Perpendicular velocity

$$v_y(t) = \frac{\Delta y(t)}{\Delta t} \tag{2}$$

Overall velocity

$$v_r(t) = \frac{\sqrt{\Delta x(t)^2 + \Delta y(t)^2}}{\Delta t} \tag{3}$$

The absolute values of $v_x(t)$, $v_y(t)$, and $v_r(t)$ at different time points were averaged respectively for all cells on a given substrate to obtain the representative parallel, perpendicular, and overall velocities. Cells that died, underwent mitosis, moved out of the imaging area, or collided with each other during the observation period were excluded from the analysis.

2.7. Statistical analysis

Data are expressed as mean ± standard deviation (SD). Comparison is made by two-tail *t*-test. Statistically significant difference is indicated by $p < 0.01$.

3. Results and discussion

Here, the average diameter of the nanopores on the AAM was determined to be 140 nm under SEM observation, as shown in Fig. 1A. To distinguish between the effect from nanoporous structure and that from alumina surface of AAM, the flat control alumina surface was used as the control substrate in this study (Fig. 1B). EDX analysis was performed on the control alumina surface and the presence of the alumina layer was confirmed (Fig. 1C). The signal of silicon comes from the silicon wafer substrate. Fig. 1D–F show the microgrooved PDMS surface with groove widths of 10 μm, 30 μm, and 50 μm, respectively. The periodicities of the microgrooves were twice as their widths. Fig. 1G shows the nanoporous PDMS surface with 140 nm in diameter.

3.1. Influence of nanopores and microgrooves on cell morphology

Both PDMS and alumina ceramics are well known to be biocompatible, and they have been commonly used in orthopaedic application and biomimetic fabrication for years [7,21–23]. Cell morphology of BEL-7402 cells after 24-h culturing on nanoporous AAM and microgrooved PDMS was observed using SEM (Fig. 2 and Fig. 3). The flat cell culture plate, flat control alumina surface, and

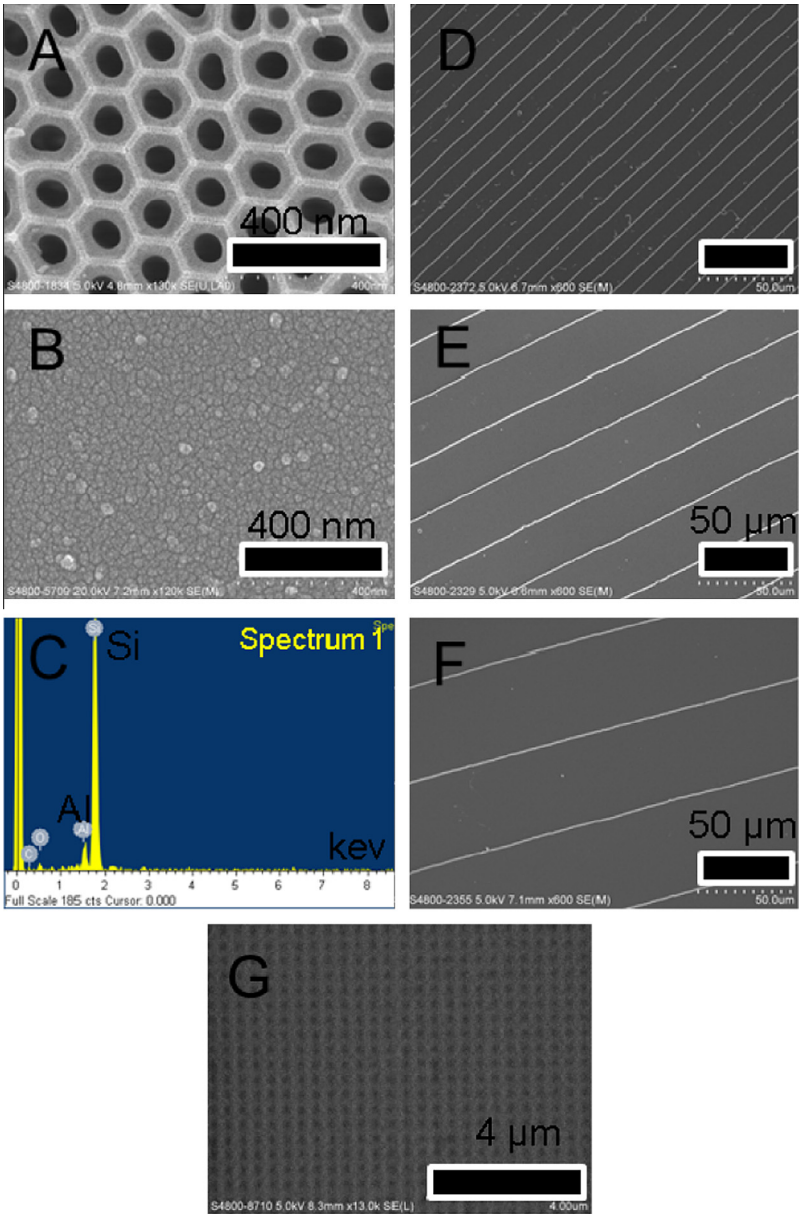

Fig. 1. Characterization of the nanoporous and microgrooved surfaces: (A) nanoporous AAM surface (140 nm), (B) control alumina surface (silicon wafer sputtered with alumina), (C) EDX spectrum of the control alumina surface, (D) 10 μm width microgrooved PDMS surface, (E) 30 μm width microgrooved PDMS surface, and (F) 50 μm width microgrooved PDMS surface. (G) 140 nm nanoporous PDMS surface.

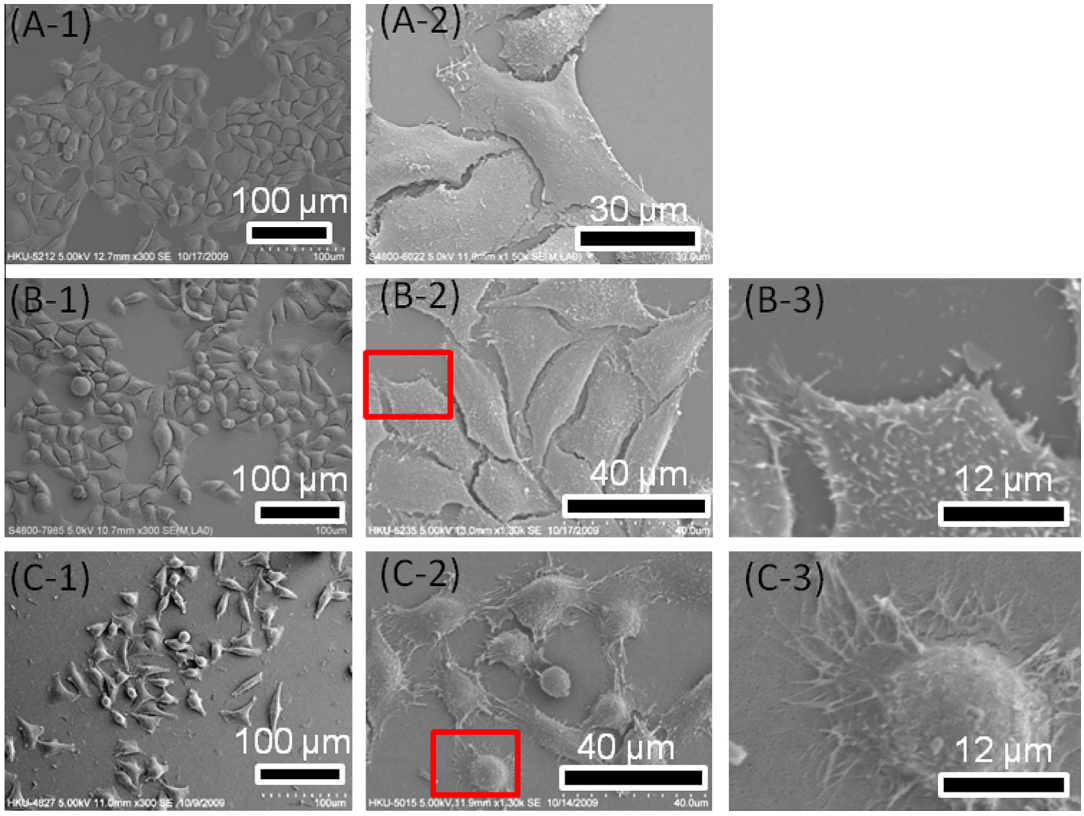

Fig. 2. Scanning electron microscopy images of the BEL-7402 cells on the cell culture plate, control alumina surface, and nanoporous AAM surface: (A-1) BEL-7402 cells on cell culture plate; (A-2) BEL-7402 cells on cell culture plate with higher magnification. (B-1) BEL-7402 cells on control alumina surface; (B-2) BEL-7402 cells on control alumina surface with higher magnification; (B-3) Selected area of BEL-7402 cell in Fig. B-2 with much higher magnification. (C-1) BEL-7402 cells on AAM (140 nm); (C-2) BEL-7402 cells on AAM (140 nm) with higher magnification; (C-3) Selected area of BEL-7402 cell in Fig. C-2 with much higher magnification.

flat PDMS served as the control substrates. The SEM images show that the BEL-7402 cells retained well-spread morphology on both the flat cell culture plate (Fig. 2A) and the control alumina surface (Fig. 2B), while the BEL-7402 formed spherical morphology on the AAM (Fig. 2C). Fig. 2B-3 and C-3 show the selected areas of BEL-7402 cell in Fig. 2B-2 and C-2 with higher magnification. Since the AAM and the control alumina surface have the same surface chemistry, this result demonstrates that the less-spread morphology of BEL-7402 on the AAM should be due to the nanoporous structure, not the chemical effect from the alumina surface. The reduced cell spreading on nanoporous structure was also observed by Park et al. where rat mesenchymal stem cells were plated on a TiO_2 nanotube surface (pore diameter >70 nm) [24]. However, although BEL-7402 cells did not spread well on 140 nm nanoporous AAM, no significant decrease in cell number was found in this study (Fig. 2C). That means 140 nm spacing reduced the cell-substrate adhesion strength of BEL-7402 cells, but did not induce the apoptosis of BEL-7402 cells. The cells on the nanoporous AAM (Fig. 2C-3) developed morphology with many more protrusions than the cells on the control alumina surface (Fig. 2B-3). Protrusion formation is an essential step during cell migration [25]. Highly migratory cells usually displayed more protrusion formation [24,26]. Thus, many protrusions appeared around the cells on the nanoporous AAM indicates that cell migration on the nanoporous surface would be easier than on the flat surface. On the other hand, the cells tend to spread spheroid on the flat PDMS (Fig. 3A) and extend along the ridges on the microgrooved PDMS (Fig. 3B–D). Compared to the cells on the flat cell culture plate (Fig. 2A), the cells on both flat PDMS and microgrooved PDMS showed less spreading. The PDMS substrate used in this study was untreated, and it has been reported that the effects from untreated PDMS on the cell spreading might depend on the cell type [1,27]. For example, the untreated PDMS does not support adhesion of vascular smooth muscle cells (VSMC), [1] but the baby hamster kidney (BHK) fibroblastic cells can be attached and well spread on it [27]. Thus, the PDMS substrate does not favour the spreading of BEL-7402 cells, which might be related to the inherent properties of the BEL-7402 cell line and the mechanism needs further studying. In addition to the effects from PDMS substrates on cell spreading, the orientations of the cells along the ridges on the microgrooved PDMS substrates are guided by the microgrooved structures. Many types of cells have also been found to exhibit the similar response to grooved substrates [2,20,28].

3.2. Characterization of cell spreading area, elongation, and orientation

Based on the optical and fluorescence microscopy images, the influence of nanopores and groove/ridge widths on cell morphology and orientation was quantified by three parameters: cell spreading area, elongation, and orientation angle (Fig. 4). The results for cells cultured on the flat cell culture plate (average area: 933.3 ± 407.1 μm^2, average elongation: 1.67 ± 0.54, average orientation angle: 48.4° ± 28.1°) and the control alumina surface (average area: 1032.6 ± 309.2 μm^2, average elongation: 1.74 ± 0.44, average orientation angle: 51.3° ± 26.9°) are not significantly different. For the nanoporous AAM substrate, the projected spreading area of the cells cultured on each substrate is significantly smaller than the cells cultured on the control alumina surface. The average projected cell area of BEL-7402 was found to be 409.6 ± 124.8 μm^2 on the nanoporous AAM and 1032.6 ± 309.2 μm^2 on the flat cell culture plate (Fig. 4A). The significant decrease of projected cell area on the

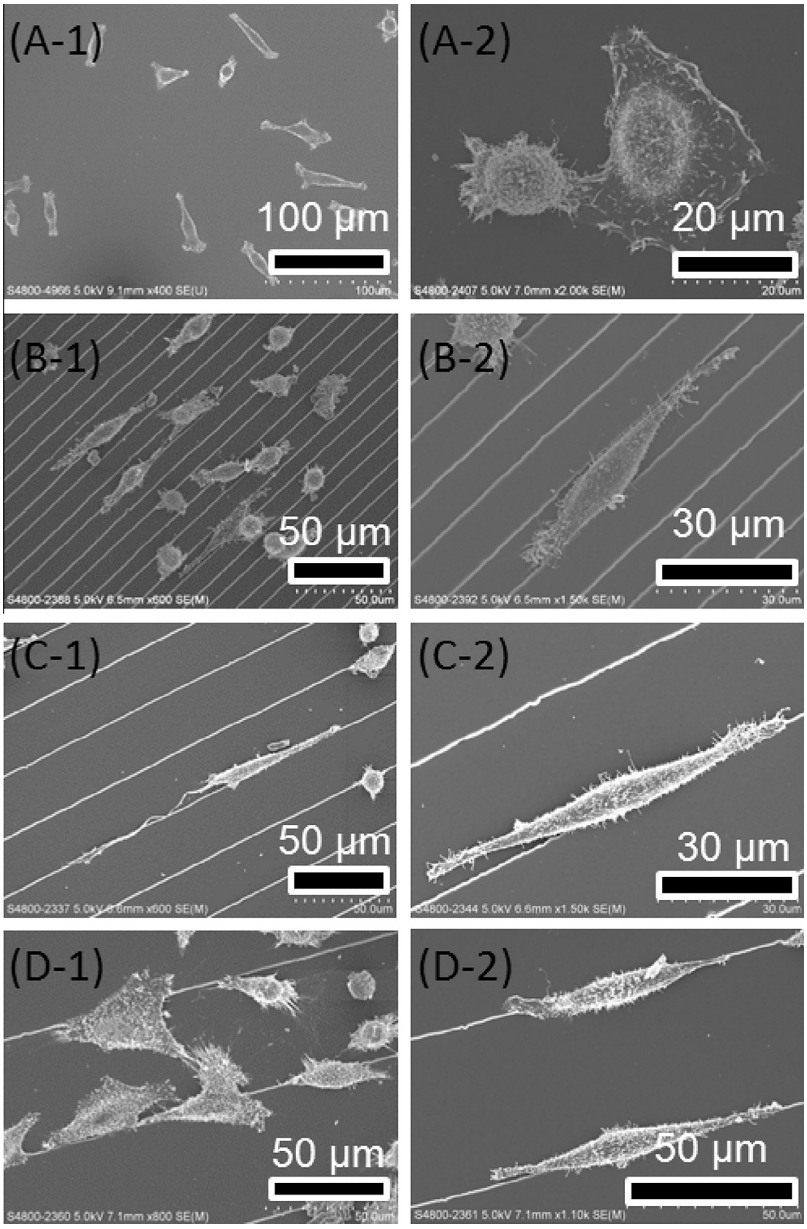

Fig. 3. Scanning electron microscopy images of the BEL-7402 cells on flat PDMS surface and microgrooved PDMS surfaces. (A-1) BEL-7402 cells on flat PDMS surface; (A-2) BEL-7402 cells on flat PDMS surface with higher magnification. (B-1) BEL-7402 cells on 10 μm width microgrooved PDMS surface; (B-2) BEL-7402 cells on 10 μm width microgrooved PDMS surface with higher magnification. (C-1) BEL-7402 cells on 30 μm width microgrooved PDMS surface; (C-2) BEL-7402 cells on 30 μm width microgrooved PDMS surface with higher magnification. (D-1) BEL-7402 cells on 50 μm width microgrooved PDMS surface; (D-2) BEL-7402 cells on 50 μm width microgrooved PDMS surface with higher magnification.

nanoporous AAM is consistent with the cell morphology changes observed from the SEM images (Fig. 2C), and it should be due to the decreased cell adhesion strength caused by the 140 nm nanoporous structures as discussed before. The smaller cell spreading area on the nanoporous surface than the flat surface was also found on the PDMS substrate when we compare the cells on the nanoporous PDMS surface (Area = 423.09 ± 73.14 μm^2) with those on the flat PDMS (Area = 599.9 ± 106.1 μm^2). As shown in Fig. 4A, the projected cell spreading area on the flat PDMS surface is significantly smaller than on the flat cell culture plate. This result is consistent with the less-spreading morphology of cells on the flat PDMS substrate observed using SEM (Fig. 3A). The projected cell area on the microgrooved PDMS surfaces is 534.1 ± 141.9 μm^2, 616.2 ± 121.2 μm^2, and 679.8 ± 162.8 μm^2 for the groove width of 10 μm, 30 μm, and 50 μm, respectively. No significant change of cell spreading area was found on all these three microgrooved PDMS substrates when compared with the cells on the flat PDMS surface (599.9 ± 106.1 μm^2). It implies that the microgrooves did not affect the cell spreading area, and the smaller spreading areas of the BEL-7402 cells on the flat PDMS substrates than on the flat cell culture plate is mainly due to the PDMS material.

Fig. 4B and C show the analysis of the cell morphology changes by studying the elongation value and orientation angle. The cells cultured on the microgrooved PDMS substrates showed stronger elongations than the cells cultured on the flat PDMS surface (Fig. 4B). The cells aligned on all the microgrooved surfaces with the average orientation angles around 7.9°, 11.8°, and 13.8° for the groove width of 10 μm, 30 μm, and 50 μm, respectively (Fig. 4C). The elongation and alignment of BEL-7402 cells on the microgrooved surfaces are also supported by the SEM images (Fig. 3B–D). The mechanism for cell elongation and alignment on the microgrooved surface was explained by the combination of

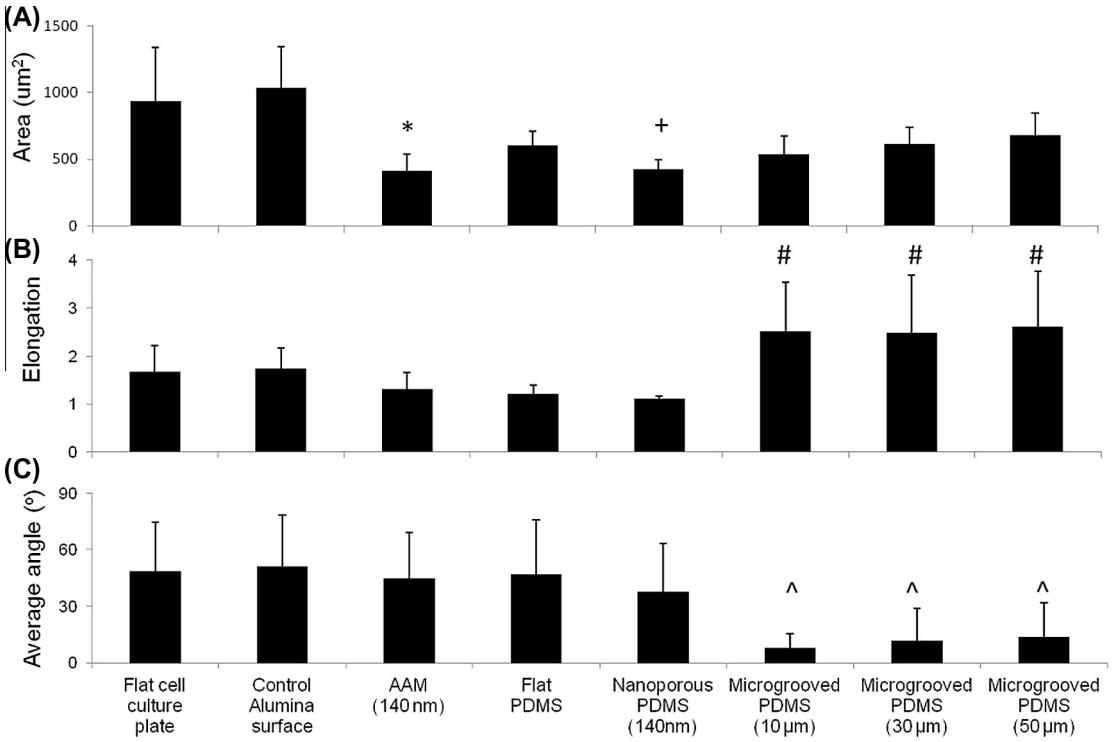

Fig. 4. Quantitative analysis of the morphology of BEL-7402 cells cultured on flat culture plate, control alumina surface, nanoporous alumina surface (AAM), nanoporous PDMS surface, flat PDMS surface, and microgrooved PDMS surfaces with different groove-widths after 24-h incubation: (A) cell spreading area, (B) cell elongation and (C) cell orientation. The grooved depth on all the groove surfaces was 2 μm. Error bar = standard error of the mean ($n = 40$). ($^{*}p < 0.001$, compared with control alumina surface; $^{+}p < 0.001$, compared with flat PDMS; $^{\#}p < 0.001$, compared with flat PDMS; $\hat{}p < 0.001$, compared with flat PDMS.).

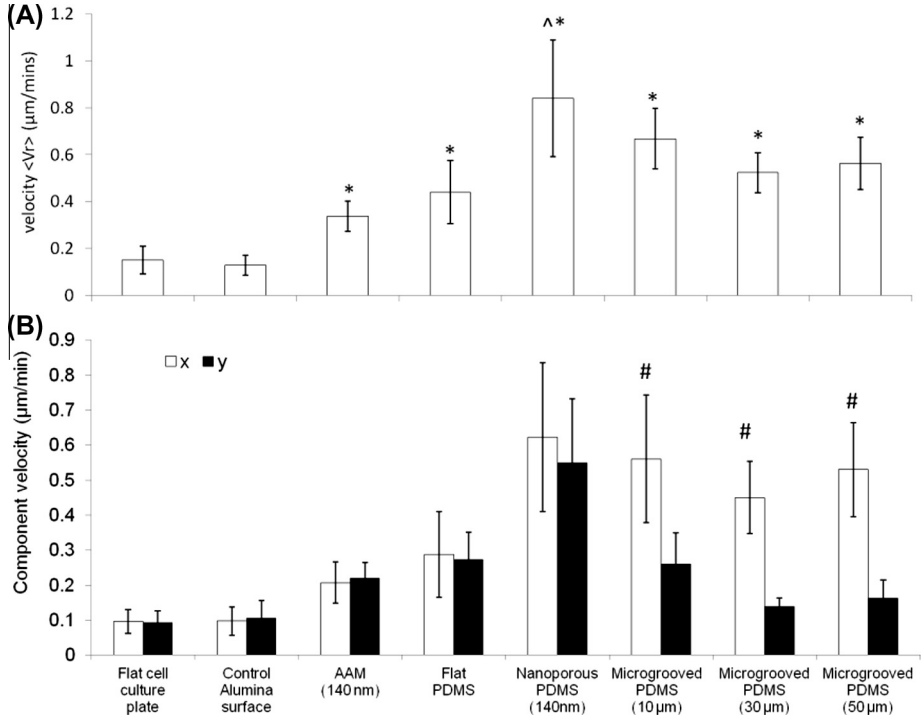

Fig. 5. Velocity of BEL-7402 cells cultured on the cell culture plate, control alumina surface, nanoporous alumina surface (AAM), flat PDMS surface, nanoporous PDMS surface and micro-grooved PDMS surfaces with different widths after 24-h incubation: (A) Overall velocity of the cells on control plates and nanoporous alumina surface, and the cells on flat PDMS surface and micro-grooved PDMS surfaces with different widths; (B) parallel (x) and perpendicular (y) component velocities of the cells on flat cell culture plate, control alumina surface and nanoporous alumina surface, and the cells on flat PDMS surface and micro-grooved PDMS surfaces with different widths. The groove depth on all the grooved surfaces was 2 μm. Error bar = standard error of the mean $n = 10$. ($^{*}p < 0.001$, compared with alumina control surface; $\hat{}p < 0.00$,compared with flat PDMS surface; $^{\#}p < 0.001$, compared with corresponding x component velocity).

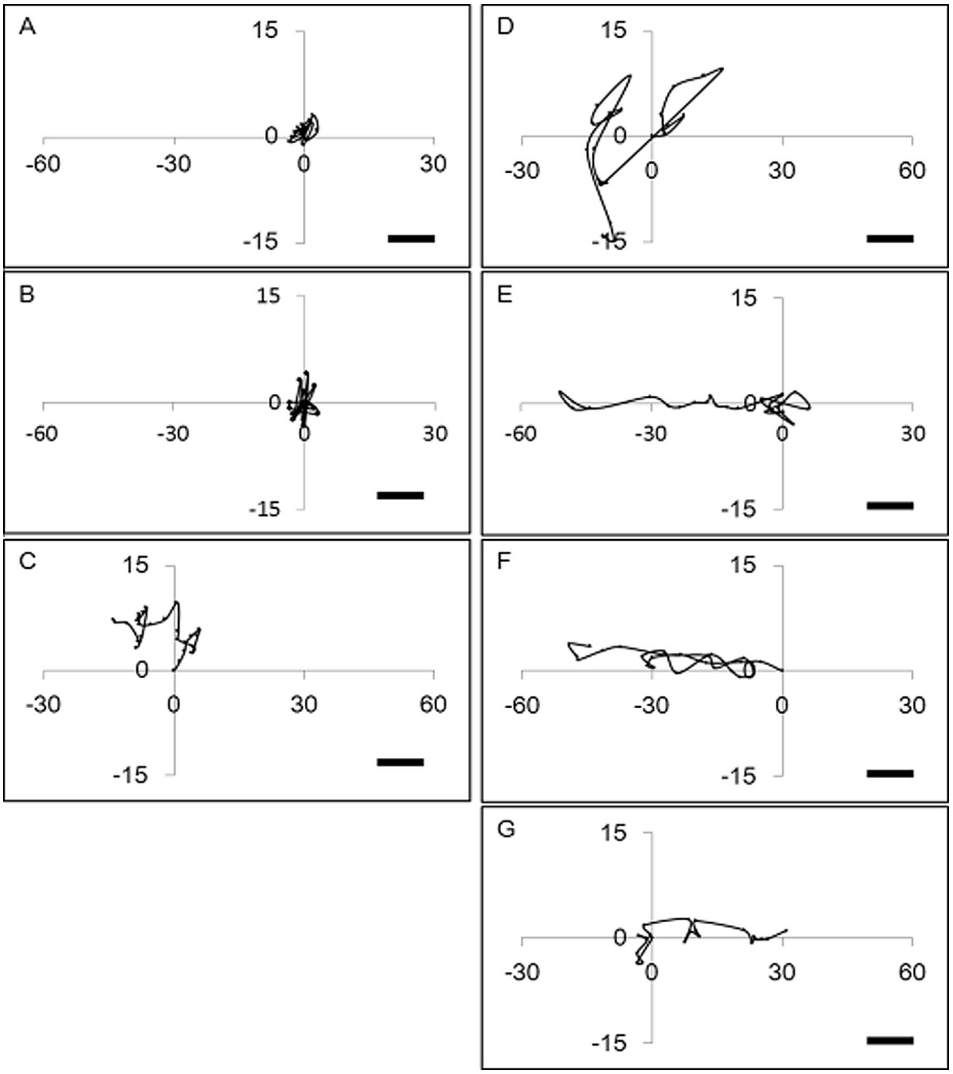

Fig. 6. Displacements of representative BEL-7402 cells over 4 h on (A) flat cell culture plate; (B) control alumina surface; (C) nanoporous AAM (140 nm in diameter); (D) flat PDMS substrate; (E) 10 μm width microgrooved PDMS substrate; (F) 30 μm width microgrooved PDMS substrate; (G) 50 μm width microgrooved PDMS substrate. In (E)–(G), the horizontal axis represents the direction parallel to the microgrooves. Scale bar, 10 μm.

promotion of cell marginal expansion along the ridges and inhibition of cell lateral expansion across the grooves [29]. This mechanism can also be applied here to explain the morphology changes of BEL-7402 cells on the microgrooved substrates. The cells on the nanoporous AAM did not show any preferred orientation, and displayed a rounded morphology. This should be due to the even distribution of nanopores on AAM, and the reduced cell-substrate adhesion of the cells on nanoporous substrate.

3.3. Characterization of cell migration speed and orientation

Cell migration of the BEL-7402 cells on the microgrooved and nanoporous surfaces were studied using time-lapse microscopy (Fig. 5). Compared to the overall velocity of cells on the flat PDMS substrate (0.44 ± 0.13 μm/min), no obvious difference was found on the overall velocities of the cells on the microgrooved PDMS surfaces, including 10 μm width microgrooved PDMS (0.67 ± 0.13 μm/min), 30 μm width microgrooved PDMS (0.52 ± 0.09 μm/min) and 50 μm width microgrooved PDMS (0.56 ± 0.11 μm/min) (Fig. 5A). The overall velocity of the BEL-7402 cells on the nanoporous AAM substrate (0.34 ± 0.06 μm/min) is significantly faster than the cells on the flat cell culture plate (0.15 ± 0.06 μm/min) and the cells on the control alumina surface (0.13 ± 0.04 μm/min). Similar effect was found when comparing the **c**ells on the nanoporous PDMS surface (0.84 ± 0.25 μm/min) and the cells on the flat PDMS (0.44 ± 0.13 μm/min). The inverse relation between cell migration speed and cell adhesion strength on various surfaces were observed and reported previously [30–32]. Hence, the increased overall velocities of the cells on the nanoporous AAM and the nanoporous PDMS should be attributed to the nanoporosity of the substrate surfaces. The cells showed weaker adhesion on nanoporous surfaces, and the weaker cell adhesion strength induced less spreading area of the cells, which is consistent with the results shown in Fig. 4A. This means the BEL-7402 cells on the 140 nm nanoporous structure can achieve sufficient adhesion strength to maintain substrate contact, but not to the extent that inhibiting the release of contacts. Thus, the nanoporosity is responsible for the loss of adhesion and increased velocity.

There was no difference between the *x*-axis and *y*-axis cell velocities on the flat cell culture plate (*x* direction: 0.10 ± 0.03 μm/min, *y* direction: 0.10 ± 0.04 μm/min), control alumina surface (*x* direction: 0.10 ± 0.04 μm/min, *y* direction: 0.11 ± 0.05 μm/min), flat PDMS (*x* direction: 0.29 ± 0.12 μm/min, *y* direction: 0.27 ± 0.08 μm/min), nanoporous AAM (*x* direction: 0.21 ± 0.06 μm/min, *y* direction: 0.22 ± 0.05 μm/min), and nanoporous PDMS (*x* direction: 0.62 ± 0.21 μm/min, *y* direction: 0.55 ± 0.18 μm/min) as shown in Fig. 5B.

From the displacements of the representative cells (Fig. 6), the cells on the nanoporous AAM surface migrate without preferred orientation (Fig. 6C). This is similar to the cells on the flat cell culture plate (Fig. 6A), the control alumina surface (Fig. 6B), and the flat PDMS (Fig. 6D) because of no directional cues on these surfaces. For BEL-7402 cells on all the microgrooved PDMS substrates, including 10 μm microgrooved PDMS (x direction: 0.56 ± 0.18 μm/min, y direction: 0.26 ± 0.09 μm/min), 30 μm microgrooved PDMS (x direction: 0.45 ± 0.10 μm/min, y direction: 0.14 ± 0.02 μm/min) and 50 μm microgrooved PDMS (x direction: 0.53 ± 0.13 μm/min, y direction: 0.16 ± 0.05 μm/min), the velocities parallel to the grooves (x direction) were higher than the velocities perpendicular to the grooves (y direction). The tendency of cell migration along the grooves was also found in other cell-groove interaction studies [16,33]. These results show that cells change their migration patterns in response to the microgrooved substrates by moving along the direction of the topography (Fig. 6E–G). We hypothesize that BEL-7402 cells respond to topography by orienting without altering their motility machinery, which is similar to the Schwann Cell [34], thus the cell movement is directional but its mechanism, including actin-based cytoskeletal dynamics, is not fundamentally altered. This would explain that the BEL-7402 cells on the microgrooved PDMS surface migrated along the grooves direction, and maintained almost the same overall migration speed as the BEL-7402 cells on the flat PDMS.

4. Conclusion

Substratum effect of micro-/nano-structured surfaces on hepatic cells was studied. Our results show that BEL-7402 cell spreading area was smaller and cell migration speed was higher on the nanoporous surfaces (140 nm in diameter) than on the flat substrates, while the cell elongation and angle were similar on both kinds of surfaces. This result implies that nanoporous structures favour BEL-7402 to exhibit sufficient adhesion strength, but not to the extent that inhibiting the release of contact. On the other hand, BEL-7402 cells on microgrooved surfaces developed an elongated morphology along the grooves, and migrated along the groove direction on all the microgrooved surfaces with different width. There were no significant differences on the cell spreading area and overall migration speed comparing the cells on the microgrooved surfaces to the cells on the flat PDMS. The results indicate that BEL-7402 cells respond to the microgrooved structures by orienting along the grooves without altering their spreading area and overall migration speed. There was no obvious pattern observed between the cell behaviour of BEL-7402 cells and the groove width at microscale. In summary, our results presented herein show that the nanoporous and microgrooved structures exhibit totally different influences on the cell morphology and migration behavior of hepatic cell line. These findings are highly conducive to tissue engineering research and medical implant design.

Acknowledgments

We would like to acknowledge the following funding agencies: PolyU Grant No: J-BB9P, G-YM43, HKU EEE Startup Fund, HKU Seed Funding for Basic Research Project No: 10400248, HKU SPACE/ Research Fund Project No. 2004912, RGC-GRF grants (HKU 704911P, PolyU 523209E), and University Grants Committee of Hong Kong (Contract No. AoE/P-04/08). We specially thank Gilly Chen (Department of Physics, Hong Kong Baptist University) and staffs from Electron Microscope Unit (The University of Hong Kong) for their technical support. We are grateful for the proofreading of our manuscript by Chris Roberts.

References

[1] X.Q. Brown, K. Ookawa, J.Y. Wong, Biomaterials 26 (2005) 3123–3129.
[2] M.J. Dalby, M.O. Riehle, S.J. Yarwood, C.D.W. Wilkinson, A.S.G. Curtis, Exp. Cell Res. 284 (2003) 272–280.
[3] P. Clark, P. Connolly, A. Curtis, J. Dow, C. Wilkinson, Development 108 (1990) 635–644.
[4] F. Braet, E. Wisse, Comp. Hepatol. 1 (2002) 1.
[5] Christopher J. Bettinger, R. Langer, Jeffrey T. Borenstein, Angew. Chem. Int. Ed. 48 (2009) 5406–5415.
[6] R.G. Flemming, C.J. Murphy, G.A. Abrams, S.L. Goodman, P.F. Nealey, Biomaterials 20 (1999) 573–588.
[7] N. Pereira-Rodrigues, P. Poleni, D. Guimard, Y. Arakawa, Y. Sakai, T. Fujii, PloS one 5 (2010) e9667.
[8] A. Hoess, A. Thormann, A. Friedmann, H. Aurich, A. Heilmann, Adv. Eng. Mater. 12 (2010) B269–B275.
[9] K.-L. Eckert, M. Mathey, J. Mayer, F. Homberger, P. Thomann, P. Groscurth, E. Wintermantel, Biomaterials 21 (2000) 63–69.
[10] E. Leclerc, Y. Sakai, T. Fujii, Biochem. Eng. J. 20 (2004) 143–148.
[11] J. Park, F. Berthiaume, M. Toner, M.L. Yarmush, A.W. Tilles, Biotechnol. Bioeng. 90 (2005) 632–644.
[12] M. Ni, W.H. Tong, D. Choudhury, N.A.A. Rahim, C. Iliescu, H. Yu, Int. J. Mol. Sci. 10 (2009) 5411–5441.
[13] D.M. Hoganson, H.I. Pryor, I.D. Spool, O.H. Burns, J.R. Gilmore, J.P. Vacanti, Tissue Eng. Part A 16 (2010) 1469–1477.
[14] K.C. Popat, E.E. Leary Swan, V. Mukhatyar, K.-I. Chatvanichkul, G.K. Mor, C.A. Grimes, T.A. Desai, Biomaterials 26 (2005) 4516–4522.
[15] M. Karlsson, E. Pålsgård, P.R. Wilshaw, L. Di Silvio, Biomaterials 24 (2003) 3039–3046.
[16] B.-Y. Yu, P.-H. Chou, Y.-M. Sun, Y.-T. Lee, T.-H. Young, J. Membr. Sci. 273 (2006) 31–37.
[17] R. Chen, D. Zhu, X. Ye, D. Shen, R. Lu, Sci. Sinica 23 (1980) 236.
[18] A. Hoess, N. Teuscher, A. Thormann, H. Aurich, A. Heilmann, Acta Biomater. 3 (2007) 43–50.
[19] A.I. Teixeira, G.A. Abrams, P.J. Bertics, C.J. Murphy, P.F. Nealey, J. Cell Sci. 116 (2003) 1881–1892.
[20] J.Y. Yang, Y.C. Ting, J.Y. Lai, H.L. Liu, H.W. Fang, W.B. Tsai, J. Biomed. Mater. Res. A 90 (2009) 629–640.
[21] E.K.F. Yim, R.M. Reano, S.W. Pang, A.F. Yee, C.S. Chen, K.W. Leong, Biomaterials 26 (2005) 5405–5413.
[22] W.-T. Su, Y.-F. Liao, I.M. Chu, Micron 38 (2007) 278–285.
[23] M. Bélanger, Y. Marois, Biomaterials 58 (2001) 467–477.
[24] J. Park, S. Bauer, K. von der Mark, P. Schmuki, Nano Lett. 7 (2007) 1686–1691.
[25] M. Bergert, S.D. Chandradoss, R.A. Desai, E. Paluch, Proc. Nat. Acad. Sci. 109 (2012) 14434–14439.
[26] H. Gerhardt, M. Golding, M. Fruttiger, C. Ruhrberg, A. Lundkvist, A. Abramsson, M. Jeltsch, C. Mitchell, K. Alitalo, D. Shima, J. Cell Biol. 161 (2003) 1163–1177.
[27] M.T. Khorasani, H. Mirzadeh, Colloids Surf., B 35 (2004) 67–71.
[28] A.I. Teixeira, P.F. Nealey, C.J. Murphy, J. Biomed. Mater. Res. A 71 (2004) 369–376.
[29] G. Dunn, A. Brown, J. Cell Sci. 83 (1986) 313.
[30] C. Arregui, S. Carbonetto, L. McKerracher, J. Neurosci. 14 (1994) 6967–6977.
[31] Y. Furuta, S. Kanazawa, N. Takeda, K. Sobue, N. Nakatsuji, S. Nomura, J. Fujimoto, M. Okada, S.A. Tadashi Yamamoto, Nature 377 (1995) 539–544.
[32] X. Zhu, J. Chen, L. Scheideler, T. Altebaeumer, J. Geis-Gerstorfer, D. Kern, Cells Tissues Organs 178 (2004) 13–22.
[33] W.-C. Chen, C.-H. Hsieh, C.-H. Li, Y.-C. Tseng, K.-M. Wang, M.-L. Yeh, in: IEEE International Conference on IEEE 2011, 2011 pp. 483–486.
[34] J.A. Mitchel, D. Hoffman-Kim, PLoS ONE 6 (2011) e24316.